Mountain snowpack response to different levels of warming

Laurie S. Huning[a,1] and Amir AghaKouchak[a,b]

[a]Department of Civil and Environmental Engineering, University of California, Irvine, CA 92697; and [b]Department of Earth System Science, University of California, Irvine, CA 92697

Edited by Glen M. MacDonald, University of California, Los Angeles, CA, and approved August 30, 2018 (received for review April 6, 2018)

Temperature variability impacts the distribution and persistence of the mountain snowpack, which critically provides snowmelt-derived water resources to large populations worldwide. Warmer temperatures decrease the amount of montane snow water equivalent (SWE), forcing its center of mass to higher elevations. We use a unique multivariate probabilistic framework to quantify the response of the 1 April SWE volume and its centroid to a 1.0 to 2.0 °C increase in winter air temperature across the Sierra Nevada (United States). A 1.0 °C increase reduces the probability of exceeding the long-term (1985–2016) average rangewide SWE volume (15.7 km^3) by 20.7%. It correspondingly is 60.6% more likely for the centroid to be higher than its long-term average (2,540 m). We further show that a 1.5 and 2.0 °C increase in the winter temperature reduces the probability of exceeding the long-term average SWE volume by 31.0% and 41.1%, respectively, whereas it becomes 79.3% and 89.8% more likely that the centroid will be higher than 2,540 m for those respective temperature changes. We also characterize regional variability across the Sierra Nevada and show that the northwestern and southeastern regions of the mountain range are 30.3% and 14.0% less likely to have 1 April SWE volumes exceed their long-term average for a 1.0 °C increase about their respective average winter temperatures. Overall, the SWE in the northern Sierra Nevada exhibits higher hydrologic vulnerability to warming than in the southern region. Given the expected increases in mountain temperatures, the observed rates of change in SWE are expected to intensify in the future.

snow | climate | probabilistic analysis | water resources | hydrology

Seasonal snowmelt represents a significant component of the water resources in the western United States, contributing ~53% of the total runoff (1). Among several environmental controls (e.g., temperature, solar radiation, humidity, etc.) and physiographic characteristics (e.g., elevation, slope, and aspect), temperature variability plays an important role in regulating montane snow water equivalent (SWE) (2, 3). As temperature increases in the spring and summer, water is released from its winter SWE storage as seasonal snowmelt. An estimated 70% of total runoff from mountains originates as snow (1).

Across California, Wang et al. (4) found that the average minimum winter temperature trend (1920–2015) increased faster than the maximum (1.2–1.9 °C per century vs. −0.30–1.2 °C per century, respectively). Previous studies (e.g., refs. 5–7) showed shifts in the timing of peak streamflow related to temperature variability across the mountainous western United States. Also, drought in the southwestern United States is not uncommon and is often associated with warm temperatures (8). As a result, warmer than average winters can result in lower than average SWE accumulation (9) such as during the severe 2014–2015 California drought that corresponded to anomalously low snowfall and SWE accumulation in the Sierra Nevada (10–13). Although the timing of peak SWE (5) and streamflow vary interannually, the 1 April SWE is often used as an indicator of the seasonal melt-derived runoff across the western United States (14).

Changes in SWE and their implications are critical to study in mountain ranges like the Sierra Nevada since its snowmelt provides an estimated 75% of the agricultural water for California (15) and 60% of the water resources in Southern California (16). However, existing in situ observations in such mountain ranges are generally located at low- to midelevations in clearings, which often results in a misrepresentation of the spatial distribution of SWE across a region (17). The spatial incompleteness and undersampling of high-elevation SWE poses challenges for water resources management globally. Spatially distributed snow data can be used to estimate the SWE volume and complement measurements from existing networks for decision-making. Such data can aid in understanding how the center of mass of the SWE volume or its centroid (expressed as an elevation) shifts upslope/downslope with hydrometeorological variability. If the centroid is forced to higher elevations than on average, the existing in situ network will sample less of the snowpack and the SWE volume will likely be smaller than average (i.e., less water stored for the spring and summer). We examine such relationships here.

Concern has been raised about the amount of water that may be stored in the future snowpack across the globe as temperatures are expected to continue to rise in mountainous regions (18). Bonfils et al. (19) concluded that warming across the montane western United States cannot be explained by internal climate variability alone. Through teleconnections, future warming of the Arctic sea ice may modulate large-scale atmospheric circulation that decreases precipitation across distant regions such as California (20). Hence, the Paris Agreement (21) further raises questions about the implications of a global 1.5 °C rise in temperature relative to the preindustrial level as they relate to water resources vulnerability. Additional research into the relative implications of 1.5 °C as opposed to 2.0 °C of

Significance

Across the world, the seasonal montane snowpack stores and releases substantial amounts of water annually. As the global temperature is projected to rise, it becomes increasingly important to assess the vulnerability of the mountain snowpack. We therefore turn to the historical record to understand the extent to which snow water equivalent (SWE) and its centroid respond to different levels of warming. Using a probabilistic framework, we show that even a 1.0 or 2.0 °C increase in average temperature leads to approximately a 20 to 40% increase in the likelihood of below average SWE. We also quantify changes in the distribution of the amount of SWE and where it is stored elevationally across the mountain range given warmer winters.

Author contributions: L.S.H. and A.A. designed research; L.S.H. performed research; L.S.H. analyzed data; and L.S.H. and A.A. wrote the paper.

The authors declare no conflict of interest.

This article is a PNAS Direct Submission.

[1]To whom correspondence should be addressed. Email: lhuning@uci.edu.

This article contains supporting information online at www.pnas.org/lookup/suppl/doi:10.1073/pnas.1805953115/-/DCSupplemental.

warming is warranted, since the former condition has been less widely examined (22). Such discussions motivate our study, where we characterize the vulnerability of SWE (i.e., amount and elevation of its centroid) to temperature variability across the Sierra Nevada over a historical period. Our analysis uses a historical spatially distributed snow data set and while it may provide insight into possible future SWE and temperature relationships, analysis of such relationships is left for forthcoming research.

We characterize the extent to which hydrologic variables respond to different levels of warming. We use the terms vulnerability or hydrologic "risk" to characterize changes in the likelihood that the long-term average SWE volume $\langle SWE \rangle$ will be exceeded (i.e., exceedance probability or P_e) for various winter temperature conditions. The terms are also used to quantify changes in the nonexceedance probability (P_{ne}) or probability that the SWE centroid, z_c, will be lower than its long-term average value $\langle z_c \rangle$ for those same temperatures. Herein, greater risk corresponds to a higher sensitivity of the snowpack to warming.

The driving question of this study is, To what extent does the hydrologic risk associated with the SWE volume vary rangewide and spatially across the Sierra Nevada (e.g., windward vs. leeward side, northern vs. southern basins, etc.) given a 1.0–2.0 °C increase in temperature? Using a conditional multivariate approach (*Materials and Methods*), we examine changes in the distribution of the SWE volume and centroid to break down the overarching question as follows: (*i*) What is the likelihood that the 1 April SWE volume will exceed its long-term average value given different average winter air temperatures across this maritime mountain range? (*ii*) What is the likelihood that the SWE centroid will occur at elevations lower than its long-term mean given an increase in temperature?

Sierra Nevada

We use the 90-m (gridded), daily Sierra Nevada snow reanalysis [described briefly in *Materials and Methods* and in detail by Margulis et al. (23)] to estimate the 1 April SWE volume and centroid. The average November–March (winter) air temperatures are also derived from this data set, providing physical consistency. In situ snow sensor observations were not used to derive the snow reanalysis, but rather for independent verification (10, 23). The reanalysis spans 32 water years (WYs; October–September) 1985–2016. The SWE centroid presented herein represents the centroid above 1,500 m. This elevation is the lowest provided by this data set as it is typically the lowest seasonally snow-covered elevation in the Sierra Nevada (24). During times when the snow line extends below 1,500 m, the centroid may be lower than presented here.

Across the Sierra Nevada, SWE and snowfall have strong regional and elevational signatures (refs. 2, 10, 25, and 26, etc.). To better understand the spatial variability of the hydrologic risk for various precipitation regimes in the Sierra Nevada [e.g., windward (western) vs. leeward (eastern) sides, higher (southern) vs. lower (northern) elevations, etc.], we divided the 20 basins outlined in Fig. 1*A* into four study domains: northwest (NW), southwest (SW), northeast (NE), and southeast (SE). Fig. 1*B* shows the normalized elevational distribution of the drainage area above 1,500 m, which greatly varies by region. Only ∼4% and 16% of the area in the NW and NE, respectively, is located above 2,500 m, while 36% and 48% of the area in the SE and SW is located above 2,500 m, respectively. These large areal differences contribute to the regional variability in hydrologic risk associated with the SWE volume and centroid and warming.

Evolution of the SWE Volume Centroid

Although we primarily characterize the 1 April snowpack, Fig. 1*C* presents the 32-y average time series (solid lines) and interannual variability (shaded areas) of the SWE volume centroid

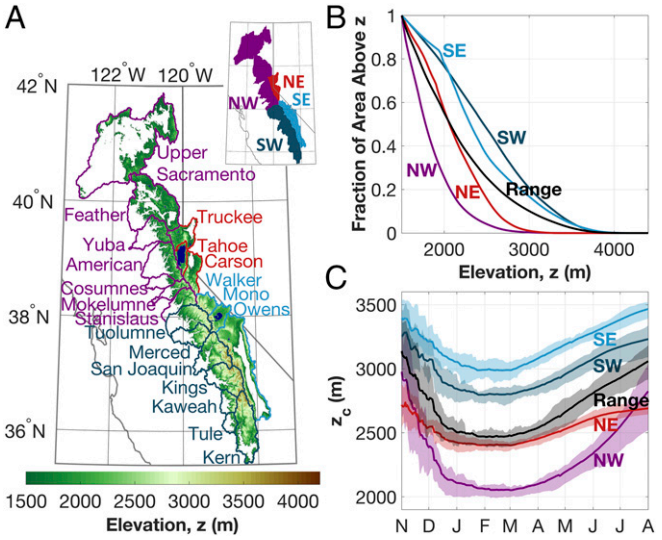

Fig. 1. (*A*) Elevation map for the Sierra Nevada above 1,500 m. Color coding denotes regionally grouped basins. This color scheme is used throughout all figures. White pixels are located below 1,500 m or outside of the study domain. (*B*) Fraction of area above each elevation (z). (*C*) Temporal movement of the SWE volume centroid (z_c). The long-term average and interquartile range of z_c are demarcated by solid lines and shaded areas, respectively. Only pixels above 1,500 m are considered in this study.

(z_c) from November to August to better understand its location on 1 April relative to other times of the year. Near the start of the accumulation season, the highest elevations receive snowfall causing the SWE volume to be located at these highest elevations. The centroid moves downslope with time as lower elevations receive snowfall and SWE accumulates over a larger area. Minimal variability occurs January–March (Fig. 1*C*), when temperatures are very cool and storms yield snowfall across nearly all elevations (10). Beginning in the spring (approximately April and May), the interannual variability of z_c begins to increase as low-elevation SWE melts and the centroid recedes toward higher elevations. SWE is again stored at higher elevations in the spring and summer until it melts. Generally, z_c takes on higher elevations in the southern Sierra Nevada (light and dark blue) than in the northern basins (purple and red) due to elevational differences (Fig. 1 *A* and *B*).

For additional perspective, we consider the most densely sampled elevations across the Sierra Nevada based on the California Department of Water Resources in situ observations (cdec.water.ca.gov/snow/current/snow/index.html). Within this network, the average snow pillow elevation is ∼2,300 m and these observations serve as an indicator of the amount of SWE across the range, rather than a direct measure of the SWE volume. Over 60% of the sensor measurements occur below 2,540 m, which is the average elevation of z_c on 1 April (Figs. 1*C* and 2). Snow courses in the Sierra Nevada have a similar elevational distribution. Thus, on average, about half of the SWE across the range is located at elevations above the majority of the sampling network. Also, not all of the basins in Fig. 1*A* have observations.

Undersampling the highest elevations with the current in situ network can misrepresent the amount of SWE stored and where its center of mass is located in space and time (Fig. 1*C*). Although high elevations make up a smaller fraction of the total area than lower elevations (Fig. 1*B*), they will play an increasingly important role in a warmer climate since warmer temperatures generally melt SWE at lower elevations resulting in a higher snow line and SWE centroid (24). Thus, the northern

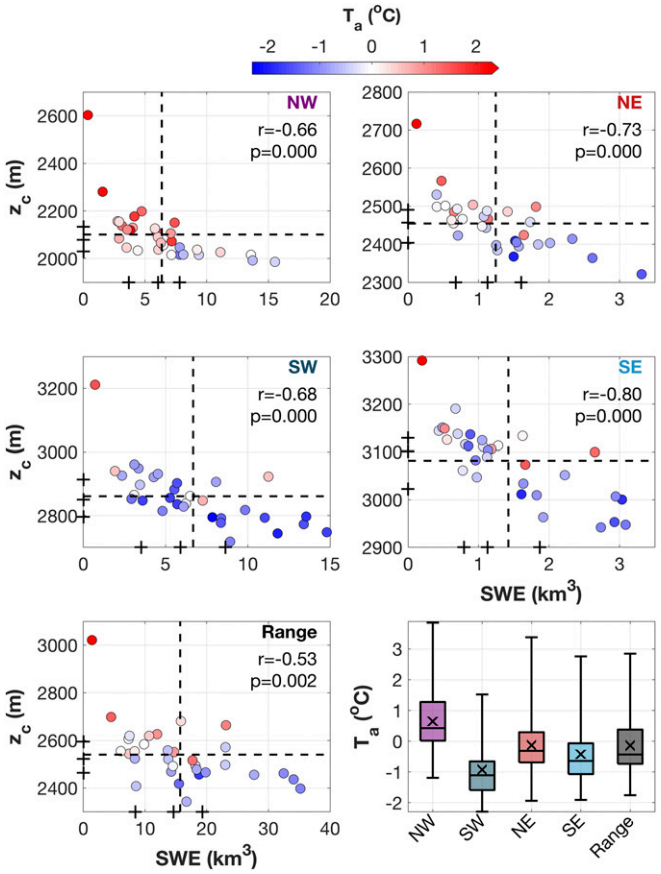

Fig. 2. Scatterplots of annual SWE volume and z_c values on 1 April where the shading of the circles represents the average winter temperature for each of the 32 y. Correlation coefficients (and *P* values) between the SWE volume and centroid are shown. Plus signs demarcate the 25th, 50th, and 75th quartiles along the respective axes. Dashed lines demarcate the long-term average values. (*Bottom Right*) Average winter temperature distribution for each region. Whiskers span the range of the data. Long-term averages are indicated with "×" symbols.

Sierra Nevada and in particular the NW, with the lowest winter SWE centroid (Fig. 1*C*), are likely most susceptible to warming. Also, the strongest correlations between winter temperature and both 1 April SWE and z_c occur in the NW (*SI Appendix*, Fig. S3). Not only do warmer temperatures shift the partitioning of total precipitation from snowfall toward rainfall, but also snow that occurs at these elevations would likely melt sooner under warmer conditions. While other hydrometeorological drivers beyond temperature (e.g., precipitation) impact SWE, the focus of this study is on understanding SWE distributions conditioned on temperature. In fact, at the highest elevations, a larger proportion of the total precipitation becomes SWE than at lower elevations.

Since water managers typically use the 1 April SWE as a metric for estimating melt-derived runoff, the remainder of this study focuses on probabilistically assessing the vulnerabilities/sensitivities of the 1 April SWE storage (amount and centroid) in relation to the average winter temperature.

SWE Volume, Centroid, and Temperature Characterization

Fig. 2 presents the regional climatology and interannual variability of the 1 April SWE volume and centroid and average winter temperature. Strong, statistically significant ($P < 0.05$) negative correlations exist between the SWE volume and z_c with the regional correlation coefficients ranging from −0.66 (NW) to −0.80 (SE). A weaker rangewide correlation exists ($r = -0.53$) due to differences among the regions (e.g., elevation) that greatly contrast between the northern and southern Sierra Nevada and degrade its strength relative to the individual regions. Nonetheless, a smaller SWE volume tends to correspond to a higher centroid elevation than when a larger SWE volume occurs.

The peak elevation of a region physically constrains the maximum possible elevation of z_c. As such, it is expected that z_c will often be lower in the northern Sierra Nevada. Warmer temperatures reduce the SWE volume, thereby increasing the height of its centroid (Fig. 2 and *SI Appendix*, Fig. S3). Stronger correlations exist between temperature and z_c than between temperature and SWE (*SI Appendix*, Fig. S3). Approximately 38% (SE) to 69% (NW) of the variance in z_c is explained by temperature variability, whereas temperature only explains ∼14% (SE) to 37% (NW) of the variance in SWE. These relationships are consistent with Mote et al. (6), who found strong correlations between the intermittent melt and the accumulated 1 April SWE in the Sierra Nevada. Regional differences in intermittent melt rates/patterns contribute to variability in the strength of the correlations. Using the Theil–Sen trend estimator, a decreasing SWE trend from WY 1985–2015 of ∼ −22 km^3 SWE per century is found, which agrees well with that of ∼ −23 and −16 km^3 per century from Wang et al. (4) (estimated using the data sets with the highest and lowest average SWE volumes from figure S7 in ref. 4 for these years, respectively).

Although 1 April is often taken to represent the end of the accumulation season, the 32-y average day-of-peak SWE across each region occurs earlier (9–16 March) with individual regions yielding extreme early (i.e., 21 December) to late (i.e., 9 May) dates for a given year. Hence, the melt season often begins before April. While our focus is on the accumulation season, other environmental controls impact the SWE distribution and melt rate and their relative importance fluctuates across seasons, mountain ranges, etc. For instance, Painter et al. (27) found that the radiative forcing by dust was a stronger control on snowmelt than temperature in the Upper Colorado River Basin.

With the western side of the mountain range facing into the prevailing winds, the NW and SW have larger average SWE volumes (dashed vertical lines in Fig. 2) than the eastern basins in the rain shadow. Corresponding to the higher mean elevation in the eastern basins (relative to the western basins, Fig. 1*B*), the NE has a higher average centroid than the NW on 1 April (Figs. 1*C* and 2). The same relationship is observed between the SE and SW. Also, the western Sierra Nevada has greater interannual variability of SWE and centroid values than the eastern regions (Fig. 2). In all regions, the extremely warm 2015 winter was the warmest winter season, which corresponded to the highest SWE centroid in the Sierra Nevada during this record. However, the coolest winter (WY 1985) neither corresponded to the largest SWE nor lowest z_c in any of the regions.

Fig. 2 (*Bottom Right*) summarizes the interannual variability of the average winter temperature. Only the NW has a positive long-term average temperature (i.e., 0.6 °C), while the other basins have subzero average temperatures ($\langle T_a \rangle$, "×" symbols), with the lowest occurring in the SW at −0.9 °C. The difference in $\langle T_a \rangle$ values between the NW and SW is ∼1.6 °C, which is 5.4 times larger than the difference between the NE and SE. While the rangewide temperatures span more than 2 °C about its mean value, this is not the case for all of the regions. Therefore, we explore the risk associated with a 1.0–2.0 °C temperature change around the rangewide average air temperature, but only consider a 1.0 °C change for the subregions.

Rangewide SWE Vulnerability to 1.0–2.0 °C Increase

Fig. 3 (*Top Left*) presents the rangewide SWE distribution sampled for various temperatures including ±0.5, ±0.75, and ±1.0 °C about the mean. These temperatures correspond to 1.0, 1.5, and 2.0 °C changes centered on $\langle T_a \rangle$, respectively. The

SWE distributions that are generated for cooler (warmer) temperatures than the 32-y average are blue (red), while the black curve denotes the SWE distribution corresponding to $\langle T_a \rangle$. The probability density functions (PDFs) become more strongly skewed toward smaller SWE values with increasing temperatures, indicating that less SWE is more probable with warmer temperatures (Fig. 3, *Top Left*). The likelihood that the long-term average SWE volume (dashed line) will be exceeded decreases with warming as Fig. 3 (*Bottom Left*) summarizes.

For a 1.0 °C change from 0.5 °C below to 0.5 °C above the mean value, it becomes 20.7% less likely that the SWE volume will be larger than its long-term average value $\langle SWE \rangle$, which corresponds to exceedance probabilities of 54.3% at −0.6 °C and 33.7% at 0.4 °C. As the temperature change about the mean increases to 1.5 and 2.0 °C, the likelihood of exceeding the average SWE further decreases. For a 1.5 °C increase (from −0.9 to 0.6 °C), it is 31.0% less likely that the long-term SWE will be exceeded, with ∼0.6 °C corresponding to an exceedance probability of 30.4%. Similarly for a 2.0 °C change, it is 41.1% less likely that the SWE volume will be larger than $\langle SWE \rangle$ when the temperature changes from −1.1 °C ($P_e = 68.4\%$) to 0.9 °C ($P_e = 27.3\%$). Therefore, the change in the exceedance probability for 2.0 °C is ∼1.3 and 2.0 times larger than for the 1.5 and 1.0 °C changes, respectively.

We similarly assess the vulnerability of the SWE centroid in Fig. 3 (*Right*) for the same temperatures. As evident in Fig. 3 (*Top Right*), the distribution of z_c shifts toward higher elevations when warmer winters occur. This shift is consistent with the inverse relationship observed in Fig. 2 between the SWE volume and its centroid, causing the PDFs in Fig. 3 (*Top Left*) to shift toward lower SWE values and those in Fig. 3 (*Top* Right) to shift toward higher elevations under warmer conditions. As a result, Fig. 3 (*Bottom Right*) shows that for the colder than average temperatures considered, the probability that the SWE centroid is lower than its 32-y average value ranges from 98.3% (at $\langle T_a \rangle - 1.0$ °C) to 82.8% (at $\langle T_a \rangle - 0.5$ °C). It drastically decreases to 22.1% at $\langle T_a \rangle + 0.5$ °C and 8.5% at $\langle T_a \rangle + 1.0$ °C for warmer than average temperatures. A temperature 1.0 °C above $\langle T_a \rangle$ is 5.8% and 13.7% less likely to have a lower than average centroid than when the winter temperature is 0.75 and 0.5 °C above $\langle T_a \rangle$, respectively. Overall, increases in the winter temperature of 1.0, 1.5, and 2.0 °C about $\langle T_a \rangle$ result in changes in the nonexceedance probabilities of −60.6%, −79.3%, and −89.8%, respectively (Fig. 3, *Right*).

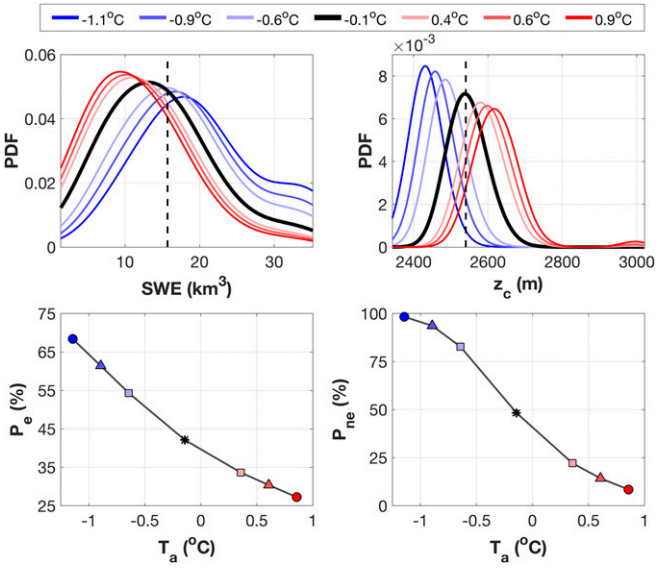

Fig. 3. Impact of 1.0, 1.5, and 2.0 °C of variability about the long-term average winter temperature in the Sierra Nevada. (*Top*) PDFs for range-wide 1 April SWE (*Left*) and z_c (*Right*) given select average winter temperatures. Dashed lines demarcate the long-term average SWE and z_c values (same as Fig. 2). Limits of *x* axes are set to the data limits. (*Bottom Left*) The likelihood that the SWE volume is larger than the long-term average SWE at different temperatures. (*Bottom Right*) The likelihood that z_c is lower than its long-term average given the same temperatures.

Under warmer atmospheric conditions, it is highly probable that the centroid will be forced to higher elevations than its long-term historical location. Also, less of the snowpack will be monitored within the existing in situ network since the centroid will likely reside above the majority of in situ sites, sampling less of the 1 April SWE distribution. Changes in the distribution of montane SWE will present new challenges for monitoring the SWE storage and forecasting the potential spring/summer runoff. These findings emphasize the importance of generating, maintaining, and improving near-real-time–distributed SWE data.

Regional Analysis

Hereafter, we consider an increase of 1.0 °C about $\langle T_a \rangle$ for each region, which represents an overall warming accounting for spatial variability. It facilitates a comparison of the vulnerability of each region to the same amount of warming by identifying areas that are the most susceptible to increased temperature and quantifying associated changes in the SWE distributions.

Regional SWE Volume Vulnerability to 1.0 °C Increase

Fig. 4 (*Left*, rows 1–4) shows the regional SWE volume distributions for the mean winter temperature (black) and 0.5 °C above (red) and below (blue) $\langle T_a \rangle$. Similar to the rangewide SWE patterns in Fig. 3 (*Top Left*), the positively skewed SWE distributions in Fig. 4 (*Left*, rows 1–4) indicate that warmer temperatures result in a higher probability of having smaller SWE volumes. For 1.0 °C of warming about the mean, the exceedance probability (Fig. 4, *Bottom Left*) decreases from 58.5% (at $\langle T_a \rangle - 0.5$ °C) to 28.2% (at $\langle T_a \rangle + 0.5$ °C) in the NW, a reduction in the likelihood of exceedance of 30.3%. For comparison, the rangewide decrease in P_e is from 54.3% to 33.7% for 1.0 °C of warming about its mean (*Bottom Left*, Figs. 3 and 4).

As shown in Fig. 4 (*Bottom Left*),1.0 °C of warming reduces the likelihood of above average SWE in the SW and SE, which have the coldest winters on average, by 17.6% and 14.0%, respectively. However, at temperatures 0.5 °C below $\langle T_a \rangle$, the SW and SE have the lowest P_e values at 53.1% and 48.2%, respectively. Overall, with warmer temperatures it becomes less probable that larger than average SWE volumes will accumulate. Consistent with previous studies (e.g., refs. 28–30), we find that the spring snowpack in the northern Sierra Nevada is more vulnerable to warming given its larger changes in exceedance probabilities than in the southern region. With lower elevations and typically warmer winters, the NW and NE, respectively, undergo changes in the exceedance probabilities of −30.3% and −28.8% highlighting their greater sensitivity to temperature. This P_e reduction from 0.5 °C below to 0.5 °C above $\langle T_a \rangle$ is also more severe along the western slope than on the eastern side (i.e., NW vs. NE and SW vs. SE).

Since all regions have average winter temperatures spanning −0.5 to +0.5 °C (Fig. 2), we also investigate the SWE response to warming across this 1.0 °C range in *SI Appendix*, *Text S1*.

Regional SWE Centroid Vulnerability to 1.0 °C Increase

As the winter temperature increases from 0.5 °C below (blue) to 0.5 °C above (red) the mean in Fig. 4 (*Right*, rows 1–4), the distribution of centroid values shifts toward the right. A shift toward higher elevations was also shown at the mountain range scale (Fig. 3, *Top Right*). Alike at the range scale, the order of the temperature-conditioned PDFs for the centroid is reversed

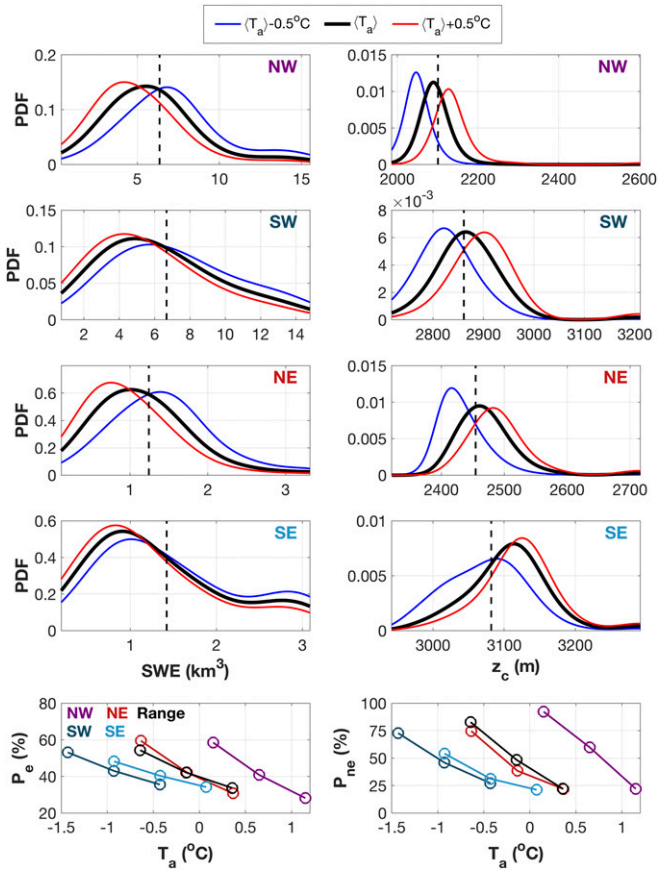

Fig. 4. PDFs for regional 1 April SWE (*Left*, rows 1–4) and z_c (*Right*, rows 1–4) given select average winter temperatures. Dashed lines demarcate the long-term average values (same as Fig. 2). Limits of *x* axes (rows 1–4) are set to the data limits in both columns. (*Bottom Left*) The likelihood that the SWE volume is larger than the long-term average SWE at different temperatures (from 0.5 °C below to 0.5 °C above of the long-term mean). (*Bottom Right*) The likelihood of z_c being lower than the long-term average centroid given the same temperature conditions. The rangewide curves in the bottom row are also shown in the bottom row of Fig. 3.

relative to those for SWE as shown in Fig. 4 (*Right* and *Left*, rows 1–4, respectively). As the snow-covered area and SWE volume are reduced with increasing temperature from 0.5 °C below to 0.5 °C above the 32-y average temperature, there is a greater chance that the center of mass of the SWE volume will be stored at higher elevations in the mountain range (i.e., the nonexceedance probability, P_{ne}, decreases).

As Fig. 4 (*Right*, rows 1–4) demonstrates, the PDFs representing the distribution of centroid values associated with a temperature of $\langle T_a \rangle$ is nearly centered on the long-term average centroid, except in the SE where the global mode of the centroid distribution for $\langle T_a \rangle - 0.5$ °C is closer to $\langle z_c \rangle$. The centroid distributions associated with $\langle T_a \rangle - 0.5$ °C and $\langle T_a \rangle + 0.5$ °C are shifted toward lower and higher elevations than $\langle z_c \rangle$, respectively. Hence the distribution of the centroid values in the SE tends to differ the most from the other regions in this respect, resulting in the SE having the lowest P_{ne} values at $\langle T_a \rangle - 0.5$ °C (Fig. 4, *Bottom Right*). The P_{ne} decreases by 33.0% in the SE for 1.0 °C of warming, whereas the decrease is >45.0% across all other regions. Although the reduction in the SE is the lowest, the P_{ne} value of 21.7%, for a temperature of 0.5 °C above the mean, is comparable to the NW, SW, and rangewide values.

Fig. 4 (*Right*, rows 1 and 5) indicates that there is a 92.3% chance that the centroid will be lower than 2,101 m when the average winter temperature is 0.1 °C (i.e., 0.5 °C below $\langle T_a \rangle$) in the NW and only a 22.0% chance at 1.1 °C, which amounts to a decrease in the P_{ne} of 70.3% for 1.0 °C of warming. As mentioned above, the change in the rangewide nonexceedance probability is also large (i.e., −60.6%) for a 1.0 °C increase from −0.6 °C. Both the NW and rangewide changes in the P_{ne} values subject to 1.0 °C of warming are substantial given the lower risks in the NE, SW, and SE, where the changes in nonexceedance probabilities are −52.8%, −45.6%, and −33.0%, respectively.

Alike the analysis for the SWE volume, we also consider a 1.0 °C change about 0 °C for the centroid in *SI Appendix*, *Text S2*.

Conclusion

As temperatures are projected to rise across California, a key question emerges: To what extent do hydrologic variables respond to different levels of warming? Hence, we characterize the range of historical snowpack responses given 1.0–2.0 °C of warming across the Sierra Nevada. The response is magnified as the amount of warming increases, which is demonstrated by it becoming less likely for the SWE volume (centroid) to be larger (lower) than its long-term average value for a 2.0 °C versus 1.5 or 1.0 °C change about the long-term mean temperature. We show that the change in the likelihood of above average SWE for a 2.0 °C change is twice as large as that for a 1.0 °C change, whereas the change in the likelihood of a lower than average SWE centroid for a 2.0 °C change is ∼1.5 times larger than for a 1.0 °C change. Although we do not use climate projections, results highlight the significance of even small changes in temperature (e.g., 1.5 °C vs. 2.0 °C of warming). Also, point-scale measurements alone cannot yield robust estimates of the montane SWE centroid as done here, which provide valuable information for water managers.

Using a multivariate approach that is adaptable to other SWE characteristics and hydrometeorological forcings, we probabilistically identify water resources vulnerabilities to provide insight into plausible SWE responses to climate change. The northern Sierra Nevada exhibits a greater susceptibility to warming than the southern portion, where the change in the likelihood of above average SWE given 1.0 °C of warming is twice as large in the NW as in the SE. The larger northern response poses risk for increased future wildfire activity given that the region has historically been vulnerable to wildfires with shifts in snowmelt timing (31). Warmer winters reduce the 1 April SWE and force its centroid to higher elevations above the majority of the in situ network, which can have major implications in water resources management, flood control, hydropower generation, etc. Given the generality of our framework, our model can be applied to other snow-covered mountain ranges across the globe.

Materials and Methods

Snow and Temperature Data. We use the SWE and air temperature maps from the Sierra Nevada snow reanalysis (23), which was generated by assimilating Landsat fractional snow-covered area images within a Bayesian framework (32) across the range. To generate the reanalysis, an ensemble of meteorological fields (e.g., air temperature, humidity, precipitation, etc.), derived from the North American Land Data Assimilation System phase 2 (NLDAS-2, ref. 33), forced the forward land surface model runs. As shown by Walton and Hall (34), the NLDAS-2 minimum and maximum temperature climatologies are biased relative to station observations. However, our modeling framework relies on relative relationships between temperature and SWE (see *Conditional Multivariate Model* below).

The posterior SWE from the snow reanalysis has been highly verified against snow pillows and courses since these observations were not assimilated (10, 23). Margulis et al. (23) found that the 1 April SWE has a mean difference (MD) and root-mean-squared difference (RMSD) less than 3 and 13 cm, respectively, relative to collocated snow pillows and courses. Huning and Margulis (10) further demonstrated that the winter cumulative snowfall derived from this data set has a MD and RMSD of −4 and 12 cm, respectively, relative to collocated snow pillows.

Conditional Multivariate Model. We use a probability risk model, similar to that described by Madadgar et al. (35), to compute the likelihood that the 1 April SWE volume exceeds its long-term average value $\langle SWE \rangle$, (i.e., $SWE > \langle SWE \rangle$) given the average winter air temperature ($T_a = t_{a1}, t_{a2}, \ldots$). Similarly, the elevation of the 1 April SWE volume centroid (z_c) is also examined. However, given the negative correlation between the SWE volume and z_c (discussed above), the exceedance and nonexceedance probabilities are computed for SWE and z_c, respectively, to maintain physical consistency. Therefore, the model computes the probability that the SWE volume will be larger than $\langle SWE \rangle$, whereas it quantifies the likelihood that the centroid of the SWE volume will be located at an elevation lower than the long-term average SWE centroid $\langle z_c \rangle$. The model utilizes region-specific thresholds to account for the various regional physiographic features (e.g., elevation) that contribute to variability of the SWE volume and z_c.

We describe the joint probability distribution between temperature T_a and the response variable Y (i.e., SWE volume or centroid) using a bivariate copula function as follows:

$$F_{T_a Y}(t_a, y) = C[F_{T_a}(t_a), F_Y(y)], \quad [1]$$

where C is the cumulative distribution function (CDF) of the bivariate copula and F_{T_a} and F_Y are marginal CDFs of T_a and Y, respectively. The copula joins multiple random variables (T_a and Y) through their marginal distributions. The conditional PDF is given by

$$f_{Y|T_a}(y|t_a) = c[F_{T_a}(t_a), F_Y(y)] \cdot f_Y(y), \quad [2]$$

where c is the PDF of the bivariate copula function and f_Y is the marginal PDF of Y. Our multivariate model depends on individual ranks of each data point (i.e., relative relationships). Copulas provide a framework for examining the underlying dependence structure of multiple variables. They serve as a mapping tool from the variable space into another space [0, 1], where the dependence structure is determined and the joint probabilities are built and then transformed back into the original/variable space (36).

We consider commonly used copula functions including Gaussian, Frank, and Clayton (36) for describing the correlation structure between variables: (*i*) SWE and T_a and (*ii*) z_c and T_a. We use a Markov Chain Monte Carlo (MCMC) sampling approach to select the model parameters following Sadegh et al. (36) for each region and pair of variables. Using this approach, we compute the maximum likelihood, Akaike and Bayesian information criteria, Nash–Sutcliff efficiency, and RMSD. The selected copulas (*SI Appendix*, Table S1) yield the most optimal values of these criteria and have a single parameter, which minimizes additional uncertainty via multiple parameters.

SI Appendix, Fig. S1 shows the posterior distribution of parameter values for the fitted copulas from the MCMC simulations, which includes uncertainty from the number of years used here. Our multivariate model is built with the parameter values corresponding to the maximum likelihood from the MCMC simulations (black line). *SI Appendix*, Fig. S2 indicates that uncertainty associated with the multivariate model parameters (*SI Appendix*, Fig. S1) results in low uncertainty in the derived conditional PDFs and probabilities for all regions. *SI Appendix*, Fig. S3 shows the data (red dots) with the conditional P_e and P_{ne} values (shading) for SWE (*Left*) and z_c (*Right*), respectively.

The snow reanalysis can be obtained from https://margulis-group.github.io/data/.

ACKNOWLEDGMENTS. This work was partially supported by the National Science Foundation Earth Sciences Postdoctoral Fellowship EAR-1725789, National Aeronautics and Space Administration Award NNX16AO56G, National Oceanic and Atmospheric Administration Award NA14OAR4310222, and the California Energy Commission Grant 500-15-005.

1. Li D, Wrzesien ML, Durand M, Adam J, Lettenmaier DP (2017) How much runoff originates as snow in the western United States, and how will that change in the future? *Geophys Res Lett* 44:6163–6172.
2. Molotch NP, Meromy L (2014) Physiographic and climatic controls on snow cover persistence in the Sierra Nevada Mountains. *Hydrol Processes* 28:4573–4586.
3. Harpold AA, Brooks PD (2018) Humidity determines snowpack ablation under a warming climate. *Proc Natl Acad Sci USA* 115:1215–1220.
4. Wang KJ, Williams AP, Lettenmaier DP (2017) How much have California winters warmed over the last century? *Geophys Res Lett* 44:8893–8900.
5. Kapnick S, Hall A (2010) Observed climate–Snowpack relationships in California and their implications for the future. *J Clim* 23:3446–3456.
6. Mote PW, Hamlet AF, Clark MP, Lettenmaier DP (2005) Declining mountain snowpack in western North American. *Bull Am Meteorol Soc* 86:39–50.
7. Cayan DR, Dettinger MD, Kammerdiener SA, Caprio JM, Peterson DH (2001) Changes in the onset of spring in the western United States. *Bull Am Meteorol Soc* 82:399–415.
8. MacDonald GM (2010) Climate change and water in Southwestern North America special feature: Water, climate change, and sustainability in the southwest. *Proc Natl Acad Sci USA* 107:21256–21262.
9. Pierce DW, Cayan DR (2013) The uneven response of different snow measures to human-induced climate warming. *J Clim* 26:4148–4167.
10. Huning LS, Margulis SA (2017) Climatology of seasonal snowfall accumulation across the Sierra Nevada (USA): Accumulation rates, distributions, and variability. *Water Resour Res* 53:6033–6049.
11. Mao Y, Nijssen B, Lettenmaier DP (2015) Is climate change implicated in the 2013-2014 California drought? A hydrologic perspective. *Geophys Res Lett* 42:2805–2813.
12. Margulis SA, Cortés G, Girotto M, Huning LS, Li D, Durand M (2016) Characterizing the extreme 2015 snowpack deficit in the Sierra Nevada (USA) and the implications for drought recovery. *Geophys Res Lett* 43:6341–6349.
13. Shukla S, Safeeq M, AghaKouchak A, Guan K, Funk C (2015) Temperature impacts on the water year 2014 drought in California. *Geophys Res Lett* 42:4384–4393.
14. Serreze MC, Clark MP, Frei A (2001) Characteristics of large snowfall events in the montane western United States as examined using snowpack telemetry (SNOTEL) data. *Water Resour Res* 37:675–688.
15. Rosenthal W, Dozier J (1996) Automated mapping of montane snow cover at subpixel resolution from the Landsat Thematic Mapper. *Water Resour Res* 32:115–130.
16. Waliser D, et al. (2011) Simulating cold season snowpack: Impacts of snow albedo and multi-layer snow physics. *Clim Change* 109:95–117.
17. Molotch NP, Bales RC (2005) Scaling snow observations from the point to the grid element: Implications for observation network design. *Water Resour Res* 41:W11421.
18. Nogués-Bravo D, Araújo MB, Errea MP, Martínez-Rica JP (2007) Exposure of global mountain systems to climate warming during the 21st century. *Glob Environ Change* 17:420–428.
19. Bonfils C, et al. (2008) Detection and attribution of temperature changes in the mountainous western United States. *J Clim* 21:6404–6424.
20. Cvijanovic I, et al. (2017) Future loss of Arctic sea-ice cover could drive a substantial decrease in California's rainfall. *Nat Commun* 8:1947.
21. UNFCCC (2015) Adoption of the Paris Agreement. Available at https://unfccc.int/resource/docs/2015/cop21/eng/l09r01.pdf. Accessed March 9, 2018.
22. Mitchell D, et al. (2016) Realizing the impacts of a 1.5 °C warmer world. *Nat Clim Chang* 6:735–737.
23. Margulis SA, Cortés G, Girotto M, Durand M (2016) A Landsat-era Sierra Nevada snow reanalysis (1985–2015). *J Hydrometeorol* 17:1203–1221.
24. Rice R, Bales RC, Painter TH, Dozier J (2011) Snow water equivalent along elevation gradients in the Merced and Tuolumne River basins of the Sierra Nevada. *Water Resour Res* 47:W08515.
25. Huning LS, Margulis SA (2018) Investigating the variability of high-elevation seasonal orographic snowfall enhancement and its drivers across Sierra Nevada, California. *J Hydrometeorol* 19:47–67.
26. Huning LS, Margulis SA, Guan B, Waliser DE, Neiman PJ (2017) Implications of detection methods on characterizing atmospheric river contribution to seasonal snowfall across Sierra Nevada, USA. *Geophys Res Lett* 44:10445–10453.
27. Painter TH, Skiles SM, Deems JS, Brandt WT, Dozier J (2018) Variation in rising limb of Colorado River snowmelt runoff hydrograph controlled by dust radiative forcing in snow. *Geophys Res Lett* 45:797–808.
28. Knowles N, Cayan DR (2002) Potential effects of global warming on the Sacramento/San Joaquin watershed and the San Francisco estuary. *Geophys Res Lett* 29:38-1–38-4.
29. Knowles N, Cayan DR (2004) Elevational dependence of projected hydrologic changes in the San Francisco estuary and watershed. *Clim Change* 62:319–336.
30. Kapnick S, Hall A (2012) Causes of recent changes in western North American snowpack. *Clim Dyn* 38:1885–1899.
31. Westerling AL, Hidalgo HG, Cayan DR, Swetnam TW (2006) Warming and earlier spring increase western U.S. forest wildfire activity. *Science* 313:940–943.
32. Margulis SA, Girotto M, Cortés G, Durand M (2015) A particle batch smoother approach to snow water equivalent estimation. *J Hydrometeorol* 16:1752–1772.
33. Xia Y, et al. (2012) Continental-scale water and energy flux analysis and validation for the North American Land Data Assimilation System project phase 2 (NLDAS-2): 1. Intercomparison and application of model products. *J Geophys Res Atmos* 117:D03109.
34. Walton D, Hall A (2018) An assessment of high-resolution gridded temperature datasets over California. *J Clim* 31:3789–3810.
35. Madadgar S, AghaKouchak A, Farahmand A, Davis SJ (2017) Probabilistic estimates of drought impacts on agricultural production. *Geophys Res Lett* 44:7799–7807.
36. Sadegh M, Ragno E, AghaKouchak A (2017) Multivariate copula analysis toolbox (MvCAT): Describing dependence and underlying uncertainty using a Bayesian framework. *Water Resour Res* 53:5166–5183.